

# Experimental and numerical study of the effect of cure cycle, tool surface, geometry, and lay-up on the dimensional fidelity of autoclave-processed composite parts

G. Fernlund<sup>a,\*</sup>, N. Rahman<sup>a</sup>, R. Courdji<sup>a</sup>, M. Bresslauer<sup>a</sup>, A. Poursartip<sup>a</sup>, K. Willden<sup>b</sup>, K. Nelson<sup>c</sup>

<sup>a</sup>Department of Metals and Materials Engineering, The University of British Columbia, 309-6350 Stores Road, Vancouver, BC, Canada V6T 1Z4

<sup>b</sup>Boeing Commercial Airplane Group, Seattle, WA 98124-2207, USA

<sup>c</sup>Boeing Phantom Works, Seattle, WA 98124-2499, USA

Received 2 November 1999; revised 11 July 2001; accepted 27 July 2001

## Abstract

Resin cure shrinkage and anisotropic thermal expansion cause process induced residual stresses in polymer composites. When relieved, the residual stresses cause reduction in enclosed angles of composite laminates; a phenomenon often called spring-in. Spring-in compromises the dimensional fidelity of composite parts and is often accounted for when designing the tool the part is made on. Spring-in is often estimated using past experience or simple analytical formulas that ignores many process parameters affecting the spring-in.

This paper presents an experimental study that shows that spring-in can be strongly affected by a number of factors such as cure cycle, tool surface, part geometry, and lay-up. The paper also shows that by developing material models that accurately represent the stress transfer between the part and the tool at the tool-part interface, and by implementing a large deformation solution technique, the experimental results observed in this study can be predicted using finite element based process models. © 2002 Elsevier Science Ltd. All rights reserved.

**Keywords:** Dimensional control; E. Prepreg; E. Tooling; B. Stress transfer

## 1. Introduction

The assembly of large composite structures in the aerospace industry requires matching of smaller sub-components in the assembly phase. Poor dimensional fidelity of the sub-components leads to increased assembly time and cost. One of the main reasons for poor dimensional fidelity of composite parts is residual stress build-up during cure, resulting in warpage when the composite part is fully cured and removed from the tool. The expected warpage of the composite part is typically compensated for in tool design using past experience, i.e. the expected warpage is 'added' to the tool geometry such that the warped part has the desired geometry. Although the concept of tool compensation is straight-forward in principle, each new part typically differs from previous parts in terms of either part and tool materials, geometry, or lay-up, making it difficult to extrapolate past experience to new parts.

The main driving forces behind residual stress build-up in the part are anisotropic thermal expansion and resin cure

shrinkage. There are several papers with experimental evidence of this presented in the literature [1–3]. Simple formulas that predict the warpage or spring-in of curved composite laminates are available in the literature [4,5], and analytical and numerical models have been developed to predict the residual stresses in cured composite parts, e.g. Refs. [6–14]. However, there are many more factors that affect the residual stress build-up and subsequent warpage.

The Composites Group at The University of British Columbia has developed COMPRO, a two-dimensional finite element code for the modeling of autoclave processing of complex composite structures [15–17]. The code is intended to include all relevant effects, including autoclave and tool characteristics, as well as material behavior. COMPRO determines component internal temperature, resin degree of cure, resin flow and the development of residual stress and deformation. The code advances previous work in a number of ways, allowing the modeling of complex two-dimensional structures with multiple composite and non-composite materials, including the effects of process tooling. A 'virtual autoclave' simulation is used to predict the boundary conditions to which parts are actually subjected during processing. In recent years, this

\* Corresponding author. Tel.: +1-604-822-3673; fax: +1-604-822-3619.  
E-mail address: goran.fernlund@ubc.ca (G. Fernlund).

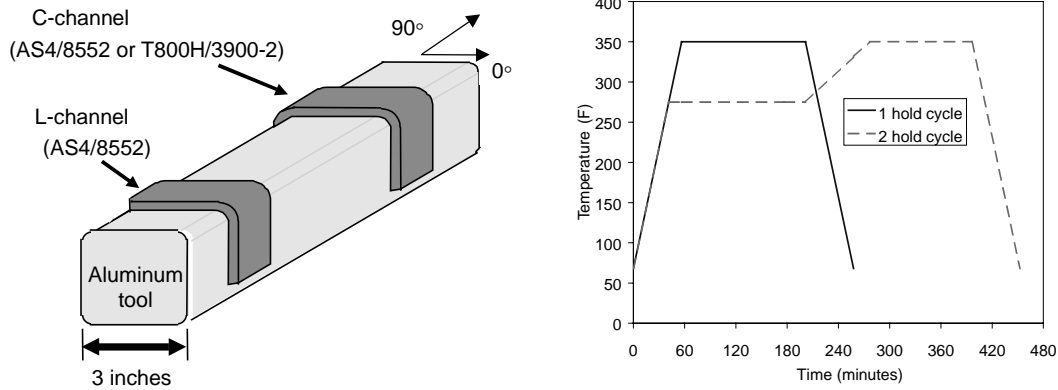


Fig. 1. Overview of specimen geometries and cure cycles.

effort has been aided considerably by funding, input, and collaboration with The Boeing Company. COMPRO is continually being improved to better describe the physics and mechanics of the manufacturing process as our knowledge grows.

This paper presents two recent improvements to COMPRO: the implementation of an updated geometry solution technique to account for large deformations, and the introduction of two new material models to better represent the mechanical interaction between the tool and the part at the tool-part interface during cure. The improved code is used to model the spring-in of carbon/epoxy L and C-channels

made on aluminum tooling. The predictions are compared to experimental results, and the effect of varying the cure cycle, tool surface, geometry, and lay-up is studied experimentally and numerically. Two different uni-directional preimpregnated fibre-reinforced plastics (prepregs), AS4/8552 and T800H/3900-2, are used in the study.

## 2. Experimental program

To study the effect of part geometry, prepreg material, lay-up, tool-surface condition, and cure cycle on the

Table 1  
Test matrix

Part number <sup>a</sup>	Material <sup>b</sup>	Shape <sup>c</sup>	Lay-up <sup>d</sup>	Tool surface <sup>e</sup> (no of layers)	Holds in cure cycle <sup>f</sup>
A-1	AS4/8552	L	[0] <sub>12</sub>	Multishield (1)	1
A-2	AS4/8552	L	[0, +45, -45, 90] <sub>2S</sub>	Multishield (1)	1
A-3	AS4/8552	L	[0, 90] <sub>6S</sub>	Multishield (1)	1
B-1	AS4/8552	C	[0, +45, -45, 90] <sub>2S</sub>	FEP (1) and Multishield (1)	1
B-2	AS4/8552	C	[0, +45, -45, 90] <sub>2S</sub>	Multishield (1)	1
B-3	AS4/8552	C	[0, +45, -45, 90] <sub>2S</sub>	Multishield (3)	1
C-1	T800H/3900-2	C	[0, +45, -45, 90] <sub>2S</sub>	FEP (1) and Multishield (1)	1
C-2	T800H/3900-2	C	[0, +45, -45, 90] <sub>2S</sub>	Multishield (1)	1
C-3	T800H/3900-2	C	[0, +45, -45, 90] <sub>2S</sub>	Multishield (3)	1
D-1	T800H/3900-2	C	[0, +45, -45, 90] <sub>2S</sub>	Multishield (3)	1
D-2	T800H/3900-2	C	[0, +45, -45, 90] <sub>2S</sub>	No release agent or FEP	1
D*-1	T800H/3900-2	C	[0, +45, -45, 90] <sub>2S</sub>	Multishield (3)	1
D*-2	T800H/3900-2	C	[0, +45, -45, 90] <sub>2S</sub>	No release agent or FEP	1
E-1	T800H/3900-2	C	[0, +45, -45, 90] <sub>2S</sub>	Multishield (3)	2
E-2	T800H/3900-2	C	[0, +45, -45, 90] <sub>2S</sub>	No release agent or FEP	2
E*-1	T800H/3900-2	C	[0, +45, -45, 90] <sub>2S</sub>	Multishield (3)	2
E*-2	T800H/3900-2	C	[0, +45, -45, 90] <sub>2S</sub>	No release agent or FEP	2

<sup>a</sup> The letter denotes the batch number and the number denotes the part number in the batch. Batches D and D\*, and E and E\*, are nominally identical and were used to study batch-to-batch variation.

<sup>b</sup> AS4/8552 and T800H/3900-2 are unidirectional carbon/epoxy prepregs.

<sup>c</sup> Fig. 2 shows the approximate dimensions of the L and C-channels shown on the tooling in Fig. 1.

<sup>d</sup> The 0° direction is defined perpendicular to the length axis of the tool (Fig. 1).

<sup>e</sup> To prevent adhesion between the part and the tool, a release coating or release ply is typically placed on the tool surface. Multishield is a liquid release agent (coating) that is wiped onto the tool, and FEP (Fluorinated Ethylene Propylene) is a thin polymer release ply. Experiments were also performed with no release agent and no release film to study what happens when the part is allowed to fully bond to the tool.

<sup>f</sup> Both one and two-hold cure cycles were used. For details, see the Appendix A.

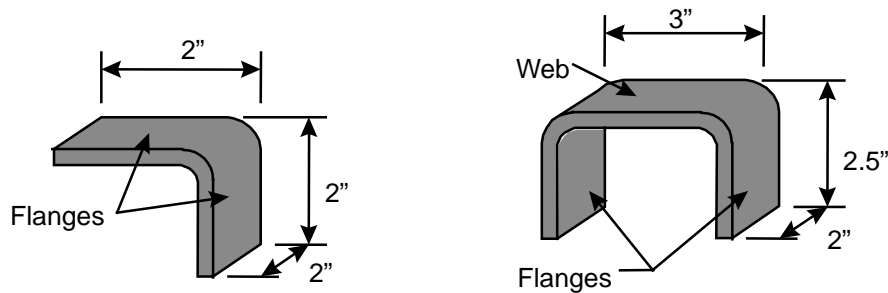


Fig. 2. Approximate dimensions of L and C-channels (all initial angles 90°).

dimensional fidelity of composite parts, a number of L and C-shaped parts were made on a small aluminum tool. Fig. 1 shows an overview of the specimen geometries and cure cycles used in the experimental program. The detailed test matrix is shown in Table 1.

### 3. Development of a material model for the tool-part interface

#### 3.1. Tool-part interaction experiments

During cure, the part and the tool want to expand or contract relative to each other because of resin cure shrinkage and differences in thermal expansion. If the tool prevents the free expansion or contraction of the part, residual stresses are built-up. The amount of constraint the tool puts on the part is influenced by part and tool geometries, part and tool stiffness, autoclave pressure, and the tool surface condition.

To measure the amount of tool-part interaction of a flat part for different tool surface conditions, a simple experiment was conducted. A rosette strain gauge was mounted on a thin aluminum tool plate, measuring the strain in the plate in two perpendicular directions. On the opposite side of the tool plate, a stack of uncured unidirectional carbon-fiber reinforced plastic (CFRP) prepreg was laid-up (Fig. 3). Two tests were performed with different tool surface conditions. In one case there were two sheets of Mylar between the tool and the part, in the other case there were no Mylar sheets and no release agent. After lay-up, the part and tool were enveloped in a vacuum bag, and heated up in an oven to 177°C. Two hours later, the part was fully cured and the

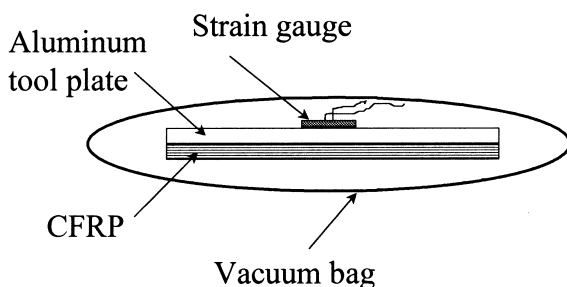


Fig. 3. Experimental set-up for flat tool-part interaction experiments.

tool-part assembly was cooled down to room temperature. The strain in the tool-plate was measured during the entire event.

Figs. 4 and 5 show the measured strain in the tool during the cure cycle. In Fig. 4, the slope of the curve is approximately  $22 \times 10^{-6}/^{\circ}\text{C}$ , which is close to the coefficient of thermal expansion (CTE) of the aluminum plate, indicating that there is little or no mechanical interaction between the part and the tool during heat-up or cool-down. Note that only the strain in the fiber direction of the prepreg is plotted in the figure. No strain measurements were taken in the transverse direction in this test. In Fig. 5 the measured strain in the fiber and the transverse direction follow the CTE of the aluminum plate up to approximately 160°C where the rate of increase drops in the fiber direction and increases slightly in the transverse direction. This is an indication of mechanical interaction between the tool and the part since the CFRP has a much lower CTE in the fiber direction and higher CTE in the transverse direction than the tool. Based on the cure kinetics of the resin and the cure cycle, the resin is expected to gel just before the hold in the cure cycle. After the part had been cured for 2 h at 177°C, the part and tool were cooled down. On the cool-down it is clearly seen that the part and tool interact with each other, resulting in a higher strain in the transverse direction and lower strain in

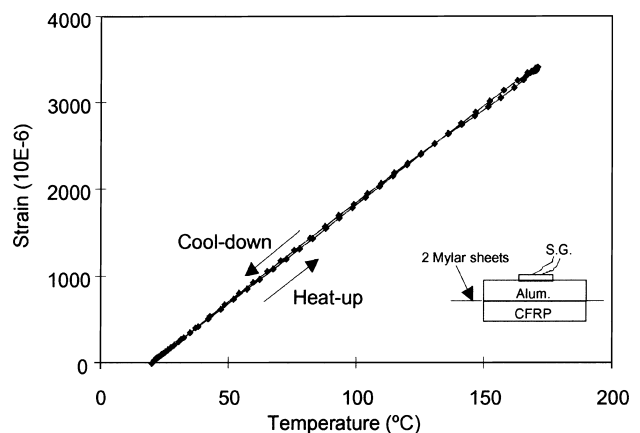


Fig. 4. Measured strain in the flat aluminum tool during heat-up and cool-down with two Mylar sheets between the tool and the part (The CFRP was uncured prior to heat-up and that the temperature was held at 177°C for two hours before cool-down).

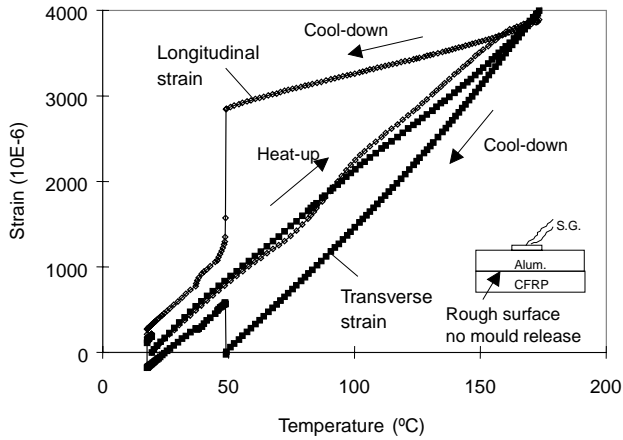


Fig. 5. Measured strain in the flat aluminum tool during heat-up and cool-down with no mould release on the tool (The CFRP was uncured prior to heat-up and that the temperature was held at 177°C for two hours before cool-down).

the fiber direction compared to the free expansion of the tool. The big drop in the measured strain at approximately 50°C on the cool-down in Fig. 5 is due to debonding of the part from the tool.

These results clearly indicate that there is little or no interaction between the tool and the part irrespective of the tool surface condition (release sheets or no release agent) prior to gelation of the resin. After gelation, however, there is little or no mechanical interaction between the tool and the part for a tool with release sheets, whereas without release agent and release sheets the part bonds to the tool and there is significant stress transfer between the tool and the part. These conclusions are only valid for flat parts. For curved parts there can be geometrical locking of the part to the tool that causes stress transfer even if the tool has a non-stick surface. This is demonstrated by experiments with L and C-channels on aluminum tooling later in the paper.

### 3.2. Finite element implementation of a tool-part interface model

The finite element formulation in COMPRO uses bilinear quadrilateral isoparametric finite elements to discretize the domain, which typically consists of both the tool and the part. The code integrates a deformation model, a heat transfer model, and a resin flow model, and uses empirical functions for the property development of the composite materials. The effect of the tool is directly modeled through simulation of the tool-part interface and tool removal [15–17].

To model the mechanical interaction between the tool and the part that was observed in the experiments above, an interface material with progressively increasing elastic modulus was introduced. The tool-part interface was modeled with a single layer of finite elements, a shear layer (Fig. 6), having transversely isotropic elastic properties.  $E_{x'x'}$  and  $G_{x'z'}$  of the shear layer (in local coordinates)

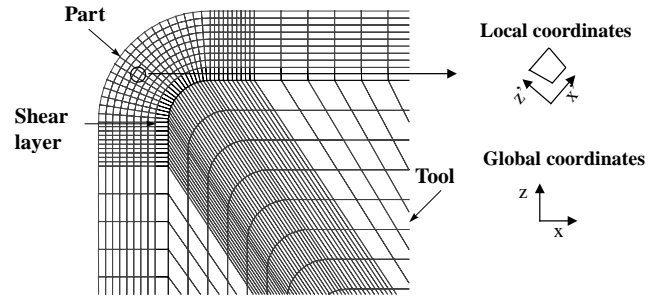


Fig. 6. Finite element mesh showing corner geometry of part, shear layer, tool, local and global coordinates.

were selected according to the condition of the tool surface. The local coordinates  $x'$  and  $z'$  are defined along the tool-part interface and perpendicular to the tool-part interface, respectively (Fig. 6). By making the shear layer stiff through the thickness (high  $E_{z'z'}$ ) and compliant in-plane (low  $E_{x'x'}$  and  $G_{x'z'}$ ), the part can 'slide' on the tool, parallel to the tool surface, but not move relative to it in the thickness direction.

A tool surface with a release agent (Multishield) or with a release ply (FEP) was represented with a soft shear layer, allowing relative movement between the composite part and the tool during the whole cure cycle. The properties  $E_{x'x'}$  and  $G_{x'z'}$  of the soft shear layer were taken as  $1.0 \times 10^3$  and  $0.38 \times 10^3$  Pa, respectively. The numbers were selected so that they are significantly lower than the modulus of the aluminum tool and the composite part, but not so low as to create numerical instabilities in the finite element solution. Varying these numbers within an order of magnitude has no effect on the solution. The transverse modulus,  $E_{z'z'}$  was the same as for the aluminum tool to prevent penetration of the part into the tool in the numerical analysis. The intention of this material model is to create a tool-part interface that does not transfer any shear stresses between the part and the tool during the entire cure cycle (Fig. 4), but at the same time prevents the part from moving away from the tool.

A tool surface with no release agent was represented with a hardening shear layer that gains stiffness during cure. The properties  $E_{x'x'}$  and  $G_{x'z'}$  of the hardening shear layer were same as that of the soft shear layer up to the gelation point of the resin in the composite part. After gelation,  $E_{x'x'}$  and  $G_{x'z'}$  were assumed to develop with the degree of cure,  $\alpha$ , similar to that of the curing resin. The final modulus of the shear layer when it is fully cured was the same as for the aluminum tool. This model is based on the assumption that a thin resin film is created between the tool and the part during cure. The intention of this material model is to create a tool-part interface that does not transfer shear stresses between the tool and the part prior to gelation but 'bonds' the part to the tool after gelation.

For both the soft and the hardening shear layer, all other properties of the shear layer (other elastic properties, thermal expansion coefficient, specific heat, and density) were taken the same as that of the tool material. At the end of the cure cycle, the shear layer was removed as a part of the tool

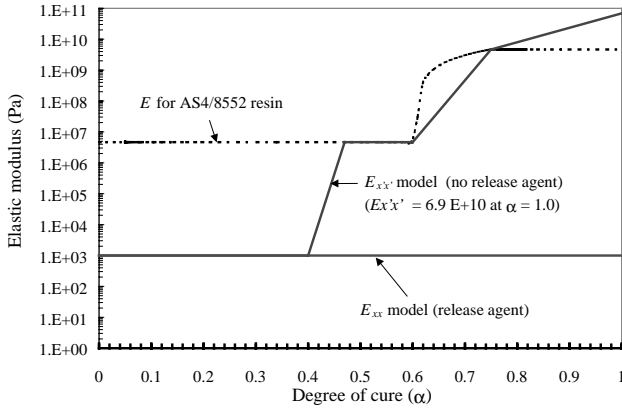


Fig. 7. Modulus development for shear layers used with AS4/8552 prepreg and aluminum tool. Dashed line represents approximate modulus development for the 8552 neat resin.

in the tool removal step of COMPRO. In this step in the finite element analysis, the constraint of the tool is removed and the residual stresses in the part are free to relax. Fig. 7 shows the modulus development for the two different shear layers used with the AS4/8552 material and the aluminum tool.

#### 4. Implementation of updated geometry solution

When a finite element model of C-channel on an aluminum tool was run on COMPRO, it was found that the finite elements representing the composite part and the tool-part interaction shear layer at and around corner areas did not deform properly with the expansion and contraction of the tool because of ‘corner locking’. Corner locking occurs mainly due to the use of initial geometry parameters at  $t = 0$  (nodal coordinates and element local axes orientation) for the calculation of element matrices at each time step of the numerical solution. The reason for corner locking in the finite element formulation of COMPRO can be explained as follows. The strain field  $\{\epsilon\}$ , the thermal and cure shrinkage strains  $\{\epsilon_0\}$ , and the autoclave pressure  $\{P\}$  are the contributors to the internal and external work considered in the current formulation, thus the total potential energy can be expressed:

$$\Pi_p = \int_{\Omega} \left( \frac{1}{2} \{\epsilon\}^T [C] \{\epsilon\} - \{\epsilon\}^T [C] \{\epsilon_0\} \right) d\Omega - \int_{\Gamma} \{u\}^T \{P\} d\Gamma \quad (1)$$

where  $[C]$  is the plane strain constitutive relations and  $\{u\}$  is the displacement field. The strain field  $\{\epsilon\}$  at any point within an element is defined in terms of the nodal displace-

ment degrees of freedom  $\{\delta\}$  as follows:

$$\{\epsilon\} = [\partial] \{u\} = [\partial][N] \{\delta\} = [B] \{\delta\} \quad (2)$$

where  $[\partial]$  is the first order differential operator,  $[N]$  is the element shape functions, and  $[B]$  contains the derivatives of  $[N]$  with respect to the global coordinate system  $(x-z)$ . By employing the principle of stationary potential energy [18], Eqs. (1) and (2) lead to the discretized finite element equilibrium equation given as:

$$\sum_{e=1}^{nele} [k]_e \{\delta\} = \sum_{e=1}^{nele} \{f\}_e \quad (3)$$

where  $[k]_e$  and  $\{f\}_e$  are the element stiffness and matrix and load vector, respectively. In the finite element formulation of COMPRO,  $[k]_e$  and  $\{f\}_e$  are evaluated in the natural coordinate system  $(\xi, \eta)$  for isoparametric elements, and a transformation from the global coordinates to the natural coordinates is performed through the Jacobian matrix  $[J]$ . Also, the constitutive relations,  $[C]$ , is a function of the composite material properties during processing and is not constant throughout the solution. As a result, the solution approach used is an incremental linear approach taking into account the update of  $[C]$  at every time step. However, no update of  $[J]$  or its components is performed. Meanwhile, the local axes orientation  $(x'-z')$  for each element is defined with respect to the global axes  $(x-z)$  using a rotation angle  $\beta$ . The angle  $\beta$  is calculated based on the nodal coordinates at  $t = 0$ , with no update after each time step. This rotation angle is used for the transformation of the local element matrices to the global coordinate system  $(x-z)$  and vice versa, and to determine boundary elements perpendicular vectors in the direction of external boundary pressure.

In the current analysis, an updated geometry solution technique was implemented by updating the Jacobian matrix  $[J]$  and its components after each time step. Following this approach,  $[k]_e$  and  $\{f\}_e$  in Eq. (3) can be written in an incremental form as:

$$[k]_e^t = \int_{-1}^1 \int_{-1}^1 [[J^{-1}]^t [B]]^T [C]^t [J^{-1}]^t [B] \det[J]^t d\xi d\eta \quad (4)$$

$$\Delta \{f\}_e^t = \int_{-1}^1 \int_{-1}^1 [[J^{-1}]^t [B]]^T [C]^t \Delta \{\epsilon_0\} \det[J]^t d\xi d\eta + \int_{-1}^1 [N]^T \{P\} \det\{J_1\}^t d\xi \quad (5)$$

where  $[B]$  in this case contains the derivatives of  $[N]$  with respect to the natural coordinate system  $(\xi, \eta)$ .  $[J]^t$  and  $\{J_1\}^t$  are the two-dimensional and one-dimensional Jacobian

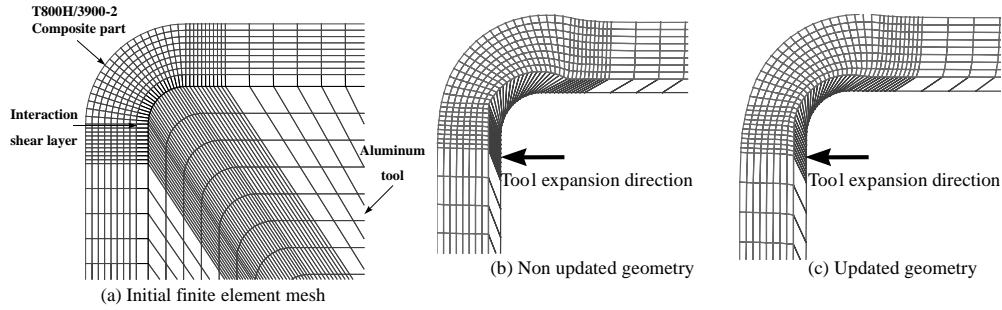


Fig. 8. Initial and deformed corner area of a channel composite part on an aluminum tool (The mesh of the tool is not included in figures (b) and (c)).

matrices, respectively, at any time  $t$  defined as:

$$[J]^t = \begin{bmatrix} \sum_{i=1,4} N_{i,\xi} x_i^t & \sum_{i=1,4} N_{i,\xi} z_i^t \\ \sum_{i=1,4} N_{i,\eta} x_i^t & \sum_{i=1,4} N_{i,\eta} z_i^t \end{bmatrix}, \tag{6}$$

$$\{J_1\}^t = \left\{ \begin{matrix} \sum_{i=1,4} N_{i,\xi} x_i^t \\ \sum_{i=1,4} N_{i,\xi} z_i^t \end{matrix} \right\}.$$

and  $x_i^t, z_i^t$  are the element nodal coordinates at time  $t$  defined as:

$$x_i^t = x_i^0 + \delta x_i^t, z_i^t = z_i^0 + \delta z_i^t \tag{7}$$

The angle  $\beta$  determining the local axes orientation ( $x^t-z^t$ ) for each element is also calculated based on the nodal coordinates at the current time  $t$ , and is used to update the local–global transformation matrices and the boundary elements perpendicular vectors.

Fig. 8(a) shows the finite element mesh at the corner area of a channel composite part on an aluminum tool with a soft shear layer. Fig. 8(b) and (c) show the predicted finite element deformations due to a horizontal thermal expansion of the tool, without and with using the updated geometry technique, respectively. It is clearly seen in Fig. 8(b) that the elements representing the soft shear layer tend to lock in their initial orientation and not deform properly with the expansion of the tool. Also, the elements representing the composite part do not shear with the expansion of the tool. This behavior would result in an erroneous prediction of the built-up residual stresses in the corner area of the composite part. Fig. 8(c) shows that corner locking has been significantly overcome by using the updated geometry technique. The difference between Fig. 8(b) and (c) is best seen by looking at the shear layer thickness and shear layer deformation at the corner. The consequences of corner locking on the residual stress state are mainly dependent on the relative thermal expansion between the tool and the composite part, the material model used for the shear layer, and the geometry of the composite part and the tool.

### 5. Finite element models for L and C-shaped composite parts

Using the updated finite element code, models of the L and C-channels in the experimental program were created and the final shape of all parts was predicted. Fig. 9 shows the finite element representation used to model the L and C-channels in the experimental program. Because of the symmetry of the C-channels about the vertical axis shown in the figure, only half the C-channel was modeled. In both finite element models, only part of the tool is included. The omitted sections of the tools have no effect on the elastic stiffness of the tool and only a relatively small effect on the thermal mass.

The boundary conditions used for the finite element models of the L and C-channels were as follows (Fig. 9). For more detail on the physical significance, see Ref. [17]:

*Heat transfer.* A convective boundary condition was applied on the external boundaries of the composite part (B1, B3, and B5) and the sides of the tool (B4 and B6). An adiabatic boundary condition was applied on the inside boundary of the tool (B2).

*Resin flow.* An impermeable boundary condition was

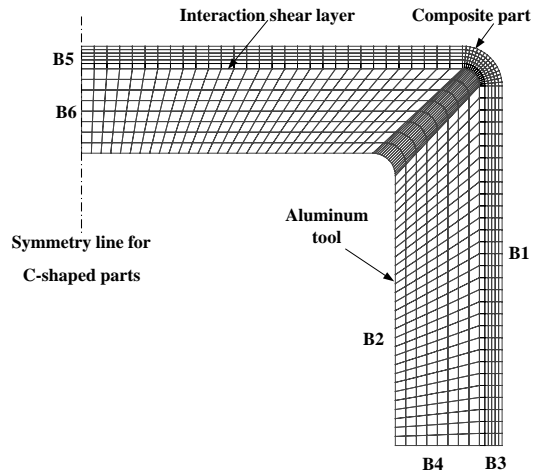


Fig. 9. A Finite element mesh for L and C-channels experiments (tool and part).

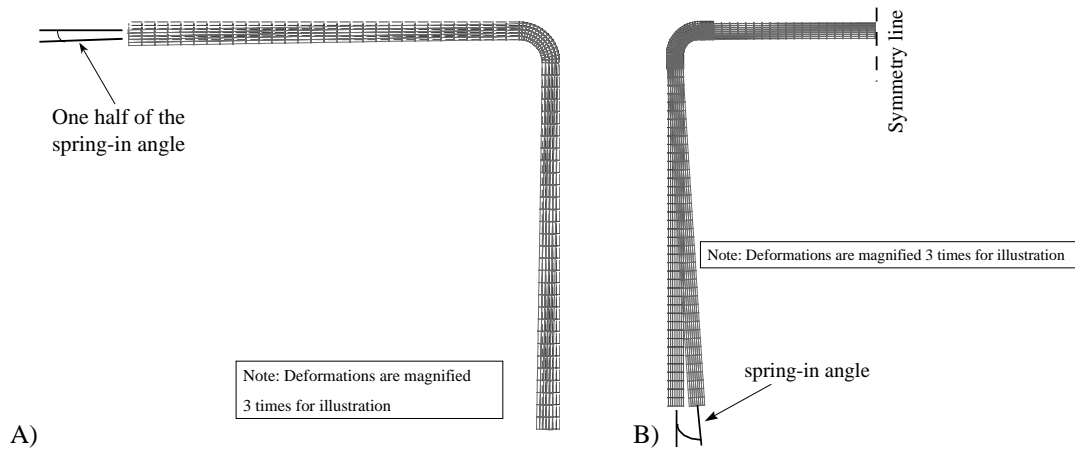


Fig. 10. Initial and deformed shape of FE models of (A) L-channels and (B) C-channels.

applied to all boundaries to simulate a ‘no-resin flow’ condition.

**Mechanical, cure cycle.** The external boundary of the composite part (B1) was subjected to autoclave pressure. The tool boundaries (B4 and B6) were set to slide along their axes. Boundary B2 is free, no pressure or displacement is prescribed.

**Mechanical, tool removal.** For the L-channel, all nodes but one along a line passing through the part corner were set to slide; this single node was fixed to prevent free-body motion. For the C-channel model, the same condition was applied at the symmetry line of the part rather than at the corner.

The process related material properties cure kinetics, modulus development, resin cure shrinkage, and thermal expansion that are required inputs for COMPRO are

available in the open literature for AS4/8552 [15] whereas for T800H/3900-2, the property database used is proprietary to The Boeing Company.

COMPRO generates a substantial amount of data at every node and element in the finite element model throughout the cure cycle. In the present case we are interested in the final shape of the parts, after the tool has been removed and residual stresses relaxed. By qualitatively examining the deformed finite element meshes after tool removal (Fig. 10), it is seen that the main predicted deformation mode is flange spring-in.

## 6. Comparison of experimental and finite element results

Examination of all the parts made showed that the main

Table 2  
Measured and predicted spring-in angles for L and C-shaped parts

Part number	Material	Shape	Lay-up	Tool surface (no of layers)	Holds in cure cycle	Measured spring-in <sup>a</sup> (°)	Predicted spring-in <sup>b</sup> (°)
A-1	AS4/8552	L	[0] <sub>12</sub>	Multishield (1)	1	1.06 ± 0.01	0.87 ± 0.05
A-2	AS4/8552	L	[0, +45, -45, 90] <sub>2S</sub>	Multishield (1)	1	1.22 ± 0.01	0.88 ± 0.05
A-3	AS4/8552	L	[0, 90] <sub>6S</sub>	Multishield (1)	1	1.09 ± 0.01	0.78 ± 0.05
B-1	AS4/8552	C	[0, +45, -45, 90] <sub>2S</sub>	FEP (1) and Multishield (1)	1	1.41 ± 0.01	1.05 ± 0.05
B-2	AS4/8552	C	[0, +45, -45, 90] <sub>2S</sub>	Multishield (1)	1	1.47 ± 0.05	1.05 ± 0.05
B-3	AS4/8552	C	[0, +45, -45, 90] <sub>2S</sub>	Multishield (3)	1	1.45 ± 0.09	1.05 ± 0.05
C-1	T800H/3900-2	C	[0, +45, -45, 90] <sub>2S</sub>	FEP (1) and Multishield (1)	1	0.80 ± 0.03	1.25 ± 0.05
C-2	T800H/3900-2	C	[0, +45, -45, 90] <sub>2S</sub>	Multishield (1)	1	0.85 ± 0.05	1.25 ± 0.05
C-3	T800H/3900-2	C	[0, +45, -45, 90] <sub>2S</sub>	Multishield (3)	1	0.72 ± 0.06	1.25 ± 0.05
D-1	T800H/3900-2	C	[0, +45, -45, 90] <sub>2S</sub>	Multishield (3)	1	1.05 ± 0.18	1.25 ± 0.05
D-2	T800H/3900-2	C	[0, +45, -45, 90] <sub>2S</sub>	No release agent or FEP	1	0.85 ± 0.10	0.99 ± 0.05
D*-1	T800H/3900-2	C	[0, +45, -45, 90] <sub>2S</sub>	Multishield (3)	1	1.19 ± 0.20	1.25 ± 0.05
D*-2	T800H/3900-2	C	[0, +45, -45, 90] <sub>2S</sub>	No release agent or FEP	1	0.75 ± 0.16	0.99 ± 0.05
E-1	T800H/3900-2	C	[0, +45, -45, 90] <sub>2S</sub>	Multishield (3)	2	1.07 ± 0.09	1.39 ± 0.05
E-2	T800H/3900-2	C	[0, +45, -45, 90] <sub>2S</sub>	No release agent or FEP	2	1.71 ± 0.10	2.05 ± 0.05
E*-1	T800H/3900-2	C	[0, +45, -45, 90] <sub>2S</sub>	Multishield (3)	2	1.24 ± 0.07	1.39 ± 0.05
E*-2	T800H/3900-2	C	[0, +45, -45, 90] <sub>2S</sub>	No release agent or FEP	2	1.71 ± 0.10	2.05 ± 0.05

<sup>a</sup> Values for spring-in angles are given in terms of average ± (maximum value – minimum value)/2. Each part was measured a minimum of three times.

<sup>b</sup> The variability ±0.05° is based on the estimated variability in calculating the spring-in for a given deformed FE mesh.

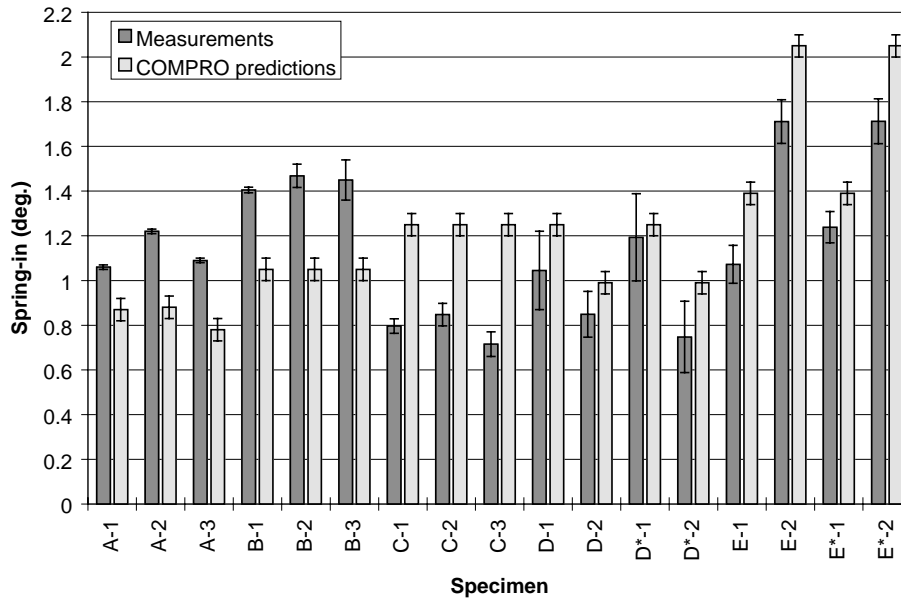


Fig. 11. Comparison of measured and predicted spring-in for L and C-channels.

type of deformation is indeed flange spring-in. Flange spring-in was measured using a digital protractor and a special measurement jig for all parts. The measurement procedure is described in detail in Appendix A. The predicted flange spring-in, using COMPRO, was calculated by evaluating the angularity between lines fitted to the deformed mesh along the tool-side of the web and the flanges, respectively. No curvature of the flanges could be observed with the naked eye, and the flanges were assumed flat for analysis purposes. Table 2 shows a summary of the measured and predicted spring-in for all specimens made in the test program. The data in Table 2 is presented in graphical form in Fig. 11 for ease of interpretation.

The following conclusions can be drawn from these results:

*Effect of lay-up.* Measurements on specimens from batch A show that the quasi-isotropic 16 ply lay-up gives the greatest spring-in, whereas the spring-in for the 12 ply unidirectional and the 12 ply cross-ply lay-up is slightly smaller. A similar trend is also seen in the COMPRO predictions.

*Effect of release agent and part geometry.* Batch B shows that the different ‘slip’ tool-surface conditions evaluated (varying number of layers of release agent and FEP) give approximately the same spring-in. However, comparison of specimen A-2 and batch B shows that the C-channels have more spring-in than the L-angles. This is likely due to the geometric locking of the C-channels on the tool, causing additional residual stress build-up because of tool thermal expansion. The COMPRO predictions agree with the measured trends although the absolute magnitude is low.

*Effect of prepreg.* Comparison of batches B and C shows that T800H/3900-2 gives less spring-in than AS4/8552.

Batch C also confirms that different slip tool-surface conditions (number of layers of release agent and FEP) have little or no effect on spring-in. The COMPRO predictions are in this case in contradiction with the measurements, predicting a higher spring-in for T800H/3900-2 than for AS4/8552.

*Effect of tool-surface condition and cure cycle.* Batches D and D\*, which are nominally identical, indicate that for a single hold cure cycle, a tool surface with release agent gives higher spring-in than a tool surface without release agent. The COMPRO predictions agree with the measured trend. Batches E and E\*, which are nominally identical, show that for a two-stage cure cycle the spring-in for a tool surface without release agent is significantly greater than with release agent. Comparison with batches D and D\* also shows that even in the case with release agent, a two-stage cure cycle gives an increase in the spring-in. Again, COMPRO predicts the measured trend. Fig. 12 shows a comparison of the average measured and average predicted flange spring-in by cure cycle and tool surface condition for the specimens in batches C, D, D\*, E, and E\*.

Table 2, Figs. 11 and 12 show that COMPRO does a good job in predicting most of the trends seen in the measurements. However, in the case of the AS4/8552 material, the predictions are low, whereas for the T800H/3900-2 material, the predictions are high. There can be many reasons why the magnitude of the predictions are off, but since the error appears to be systematic for each prepreg material, it can likely be attributed to that one of the key material properties, thermal expansion or resin cure shrinkage, are off. Note that COMPRO is a calibration free model, where the material inputs are based on materials characterization of small test coupons.

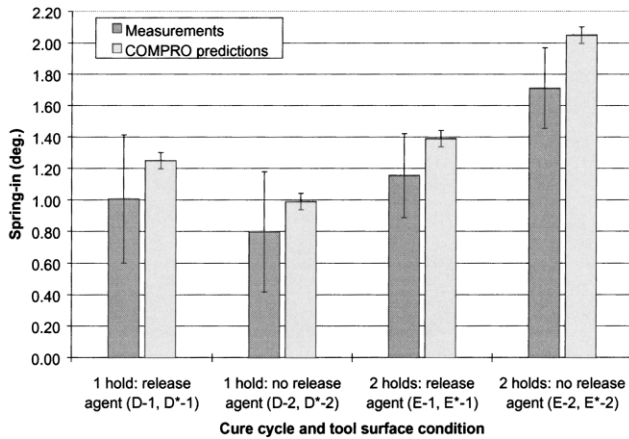


Fig. 12. Comparison of measured and predicted spring-in of C-channels made of T800H/3900-2 by cure cycle and tool surface condition.

## 7. Summary and conclusions

The main findings from the present experimental study are:

If there is a substantial amount of plies in the laminate with fibers in the direction of the curvature of the part, the amount of  $\pm 45$  and  $90^\circ$  plies have a small effect on the spring-in.

For a high CTE tooling material such as aluminum, a C-channel exhibits more spring-in than an L-channel due to the ‘geometric locking’ of the part on the tool. In the present case the spring-in was approximately 30% greater for C-channels than for L-channels.

The AS4/8552 prepreg gave approximately 50% more spring-in than the T800H/3900-2 prepreg for the quasi-isotropic C-channels made in this study.

The tool surface and the cure cycle can have a significant effect on the spring-in. In the present study with C-channels on aluminum tooling, the spring-in was 20% less for a tool with no release agent compared to a tool with release agent when the cure cycle had one hold at  $350^\circ\text{F}$ . In the case of a two hold cure cycle, with holds at  $275$  and  $350^\circ\text{F}$ , where the part was allowed to gel on the first hold, the spring-in was almost 50% greater for a tool with no release agent compared to a tool with release agent. The two hold cycle also gave a spring-in that was about 15% greater than the one hold cycle for a tool with release agent, indicating that even with release agent on the tool the ‘geometric locking’ of the part on the tool can affect the spring-in significantly.

The main findings from the present numerical study are:

Although flange spring-in in many cases is dependent on many complex factors such as tooling, cure cycle, tool-surface condition, and part geometry (geometrical locking), flange spring-in can be predicted by using a finite element based process model such as COMPRO. With the improvements to COMPRO presented in this paper, COMPRO was shown to accurately predict most experimental trends observed in this study.

## Appendix A

### A.1. Single hold cure cycle

The single hold cure cycle can be defined in five segments:

1. Pressurize the autoclave to 70 psig.
2. Heat the autoclave to  $350^\circ\text{F}$  at a ramp rate of  $5^\circ\text{F}$  per minute with a criterion temperature (the temperature the controller moves to the next segment) of  $T_{\text{lag}} = 340^\circ\text{F}$ .
3. Hold for 120 min.
4. Cool the autoclave down to a target temperature of  $60^\circ\text{F}$  until the criterion temperature of  $T_{\text{lag}} = 120^\circ\text{F}$  is reached.
5. Reduce the autoclave pressure to ambient.

Leave autoclave and part to cool down to room temperature before taking out and de-bagging the part. Fig. A1 shows a schematic of the single hold cure cycle.

### A.2. Double hold cure cycle

This cure cycle features two holds and can be defined in seven segments:

1. Pressurize the autoclave to 70 psig.
2. Heat the autoclave to  $275^\circ\text{F}$  at a ramp rate of  $5^\circ\text{F}$  per minute with a criterion temperature of  $T_{\text{lag}} = 265^\circ\text{F}$ .
3. Hold for 160 min.
4. Heat the autoclave to  $350^\circ\text{F}$  at a ramp rate of  $1^\circ\text{F}$  per minute with a criterion temperature of  $T_{\text{lag}} = 340^\circ\text{F}$ .
5. Hold for 120 min.
6. Cool the autoclave down to a target temperature of  $60^\circ\text{F}$  until the criterion temperature of  $T_{\text{lag}} = 120^\circ\text{F}$  is reached.
7. Reduce the autoclave pressure to ambient.

Leave autoclave and part to cool down to room temperature before taking out and de-bagging the part. A schematic of the double hold cure cycle is shown in Fig. A2.

### A.3. Measurement techniques

Examination of the cured parts showed that the main type

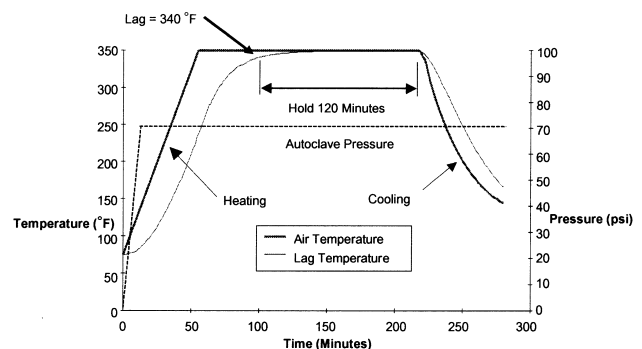


Fig. A1. Single hold cure cycle.

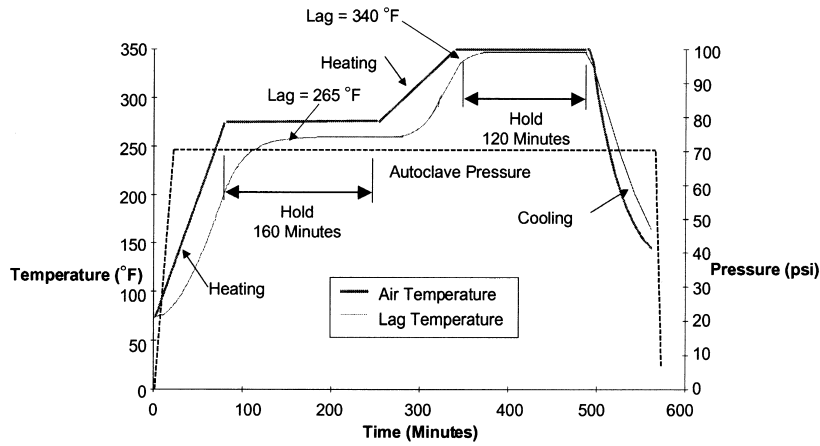


Fig. A2. Double hold cure cycle.

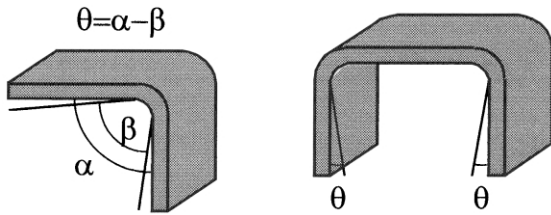


Fig. A3. Spring-in of L and C-channels.

of process induced deformation of the L and C-shaped parts were flange spring-in,  $\theta$  (Fig. A3).

Spring-in angle measurements were performed using a Mitutoyo digital protractor. A measuring aid consisting of a 6 in. long steel hinge with screws to lock the hinge at a desired angle was mounted on a flat base with three 3 in. long pins. This device was used to measure the spring-in of the L and C shaped parts. The part is first placed on the measuring aid so that it straddles the hinge. Then, using a flashlight to light the gap between the hinge face and the inside flange, the hinge is rotated until the two surfaces meet (Fig. A4(A)). The screws are tightened to lock the hinge in position and the part is removed. The digital protractor is placed on the top face of the hinge, and is zeroed.

The spring-in angle is then measured with respect to the second face on the measurement aid (Fig. A4(B)).

A.4. Lay-up and curing of L and C-channels

After the tool surface was degreased and coated with release agent, a hot air gun was used on the first ply to heat up and soften the prepreg to increase workability around the corners. Small pieces of high temperature tape were used to hold down the first ply to the tool. After the first ply was laid up on to the tool, the tool was put in a vacuum bag for debulking for approximately 10 min. Vacuum was then applied for 4–5 min after every fourth ply and upon completion of the lay-up.

In each autoclave run, four thermocouples were used to monitor temperature during the cure cycle. One thermocouple was placed on the flange edge of one of the parts, while the other two thermocouples were fixed to the tool adjacent to each of the parts. The thermocouples were held in place with high temperature tape, and where the leads lay close to the part, bleeder pads were used to cover the wires to prevent resin flow along the wires. Fig. A5 shows the location of the thermocouples for the C shaped parts.

Once the thermocouples were in place, the tool and the parts were covered with a sheet of FEP, cut to size and held in place with high temperature tape. The tool was then

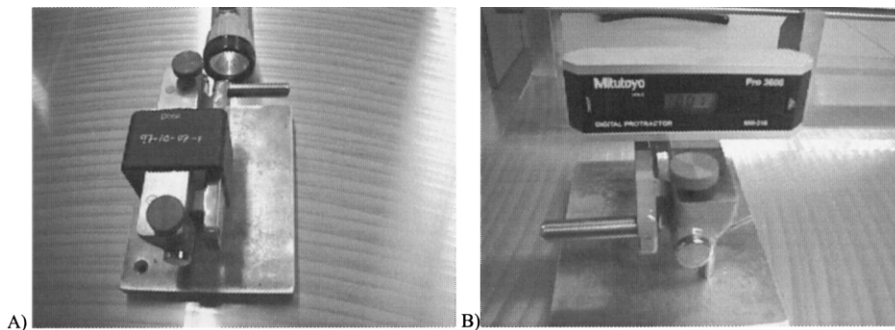


Fig. A4. (A) Measurement hinge and specimen; (B) Measurement hinge with digital protractor on top surface.

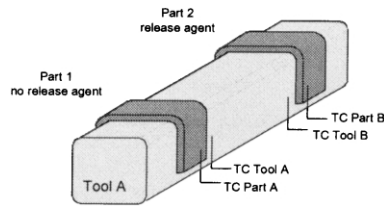


Fig. A5. Location of thermocouples.

wrapped in breather material to protect the vacuum bag from punctures caused by the edges of the tool. The breather also improved airflow during compaction by providing a airway from the tool to the vacuum port, which rested on a loosely woven mat to help keep the airway open underneath. A new vacuum bag was made and sealed with tacky tape for the curing of the part.

When the excess resin was scraped away, the parts with release agent were easily removed from the tool. In all cases, the part with no release agent was permanently bonded to the tool. The section of tool holding the bonded part was cut off with a saw. Holes were drilled through the section and the core was removed. Pliers were then used to pry away the remaining aluminum layer. Once part of the aluminum was removed from one of the flanges, the rest of the aluminum came off easily.

## References

- [1] Rennick TS, Radford DW. Components of manufacturing distortion in carbon fibre/epoxy angle brackets. 28th International SAMPE Technical Conference, 4–7 November 1996. p. 189–97.
- [2] Ridgard C. Accuracy and distortion of composite parts and tools: causes and solutions. Tooling for Composites'93, 18–19 January, Pasadena, California, 1992. EM93-113.
- [3] Stephan A, Schwinge E, Müller J, Öry H. On the springback effect of CFRP stringers: an experimental, analytical, and numerical analysis. 28th International SAMPE Technical Conference, 4–7 November 1996. p. 245–54.
- [4] Nelson RH, Cairns DS. Prediction of dimensional changes in composite laminates during cure. Thirty-fourth International SAMPE Symposium, 8–11 May, 1989. p. 2397–410.
- [5] Huang CK, Yang SY. Warping in advanced composite tools with varying angles and radii. *Compos Part A* 1997;28A:891–3.
- [6] Loos AC, Springer GS. Curing of epoxy matrix composites. *J Compos Mater* 1983;17(2):135–69.
- [7] White SR, Hahn HT. Mechanical property and residual stress development during cure of a graphite/BMI composite. *Polym Engng Sci* 1990;30(22):1465–73.
- [8] Bogetti TA, Gillespie Jr. JW. Two-dimensional cure simulation of thick thermosetting composites. *J Compos Mater* 1990;25(3):239–73.
- [9] Bogetti TA, Gillespie Jr. JW. Process-induced stress and deformation in thick-section thermoset composite laminates. *J Compos Mater* 1992;26(5):626–60.
- [10] Harper BD, Witsman Y. On the effects of environmental conditioning on residual stresses in composite laminates. *Int J Solids Struct* 1985; 21:907.
- [11] Stango RJ, Wang SS. Process-induced thermal stress in advanced fibre-reinforced composite laminates. *J Engng Ind* 1984;106(1):48–54.
- [12] White SR, Kim YK. Viscoelastic analysis of processing-induced residual stresses in thick composite laminates. *Mech Compos Mater Struct* 1997;4:361–87.
- [13] White SR, Kim YK. Process-induced stress analysis of AS4/3501-6 composite material. *Mech Compos Mater Struct* 1998;5(2):153–86.
- [14] Chen PC, Ramkumar RL. RAMPC-An integrated three-dimensional design tool for processing composites. 33rd International SAMPE Symposium, 7–10 March 1988. p. 1697–708.
- [15] Hubert P, Vaziri R, Poursartip A. A two dimensional flow model for the process simulation of complex shape composite laminates. *Int J Numer Meth Engng* 1999;44(1):1–26.
- [16] Johnston A, Vaziri R, Poursartip A. A plane strain model for process-induced deformation of composite structures. Accepted for publication.
- [17] Johnston A, Hubert P, Fernlund G, Vaziri R, Poursartip A. Process modelling of composite structures employing a virtual autoclave concept. *J Sci Engng Compos Mater* 1996;5(3–4):235–52.
- [18] Bathe KJ. Finite element procedures. New Jersey: Prentice-Hall, 1996.